Inversion of P-wave data in laterally heterogeneous VTI media. Part II: Irregular interfaces

Vladimir Grechka, Andrés Pech, and Ilya Tsvankin
Center for Wave Phenomena, Department of Geophysics, Colorado School of Mines, Golden, CO 80401-1887

ABSTRACT
P-wave reflection traveltimes may be used to constrain the depth scale of transversely isotropic models with a vertical symmetry axis (VTI), if the medium above the reflector is *laterally heterogeneous*. In Part I of this work we examined the inversion of P-wave moveout data for the vertical velocity V_{P0} and the anisotropic coefficients ϵ and δ in VTI models with planar dipping interfaces.

Here, these results are extended to VTI media composed of homogeneous layers separated by *irregular* (e.g., curved) boundaries. Despite the higher complexity of the model, non-planar interfaces increase the angle coverage of reflected rays, which helps to resolve the trade-offs between the medium parameters. Singular value decomposition (SVD) shows that there exists a subset of VTI models for which all parameters needed for anisotropic *depth* processing can be obtained solely from P-wave zero-offset reflection traveltimes and NMO ellipses. We also develop a tomographic-style inversion procedure designed to reconstruct both the interfaces and the VTI parameters and demonstrate its reliable performance on input data contaminated by noise.

SVD analysis and moveout inversion are implemented using an efficient modeling technique based on the theory of NMO-velocity surfaces generalized for wave propagation through irregular interfaces. This methodology makes multi-azimuth and multi-offset anisotropic ray tracing unnecessary because the effective NMO ellipse at the surface is obtained by computing a single (zero-offset) ray.

Key words: P-waves, VTI media, irregular intermediate interfaces

Introduction

Depth imaging in *laterally homogeneous* VTI media above the target reflector is hampered by the fact that P-wave reflection data alone cannot be used to resolve all three relevant model parameters – the P-wave vertical velocity V_{P0} and the anisotropic coefficients ϵ and δ. As discussed in more detail in Part I of this work (Grechka et al., 2000), P-wave traveltimes (including dip moveout and nonhyperbolic moveout) in such models are controlled by just two parameter combinations: the NMO velocity from a horizontal reflector $V_{\rm nmo}(0) = V_{P0}\sqrt{1+2\,\delta}$ and the anisotropic coefficient $\eta \equiv \dfrac{\epsilon-\delta}{1+2\,\delta}$. However, this result of Alkhalifah and Tsvankin (1995) is no longer valid if the overburden contains dipping interfaces or lateral velocity gradient (Grechka and Tsvankin, 1999; Le Stunff et al., 1999). Although lateral heterogeneity introduces additional unknowns to be estimated from reflection data, it may also provide information about the individual values of V_{P0}, ϵ and δ.

In Part I of this work we evaluated the feasibility of parameter estimation for VTI media composed of homogeneous layers separated by planar dipping interfaces. If the interfaces do not intersect each other, unambiguous inversion for the depth model requires minimal *a priori* information, such as knowledge of a single VTI parameter in one of the layers. Here, we study the inversion of P-wave reflection traveltimes for more complicated VTI models which contain *irregular* interfaces.

We begin with extending the theory of the NMO-velocity surfaces (Grechka and Tsvankin, 1999) to anisotropic media with irregular interfaces and developing

an efficient algorithm for modeling multi-azimuth and multi-offset reflection traveltimes. Then, we employ singular value decomposition and actual inversion of *P*-wave reflection data to show that for some VTI models with smooth curved interfaces parameter estimation in depth can be accomplished without any *a priori* information.

NMO velocity in anisotropic media with irregular interfaces

NMO velocity on a curved CMP line

Grechka and Tsvankin (1999) examined pure-mode NMO velocity recorded along CMP lines arbitrarily oriented in 3-D space. They showed that the NMO velocity $V_{\rm nmo}(\mathcal{L})$ measured in 3-D space along a CMP line specified by the unit vector $\mathcal{L}$ is given by

$$\frac{1}{V^2_{\rm nmo}(\mathcal{L})} = \mathcal{L}\,\mathbf{U}\,\mathcal{L}^{\mathbf{T}}\,, \tag{1}$$

where $\mathbf{T}$ denotes transposition. The 3×3 symmetric matrix $\mathbf{U}$ is expressed in terms of the spatial derivatives of the one-way traveltime τ or the slowness vector $\mathbf{p}$:

$$U_{km} = \tau_0\,\left.\frac{\partial^2\tau(\mathbf{x})}{\partial x_k\,\partial x_m}\right|_{\mathbf{x}=\mathbf{Y}} = \tau_0\,\left.\frac{\partial p_k(\mathbf{x})}{\partial x_m}\right|_{\mathbf{x}=\mathbf{Y}}, \qquad (k,m=1,2,3)\,. \tag{2}$$

Here τ_0 is the one-way zero-offset traveltime, and the derivatives are evaluated at the CMP location $\mathbf{x}=\mathbf{Y}$.

The matrix $\mathbf{U}$ describes a quadratic *NMO-velocity surface* obtained by plotting NMO velocity as the radius-vector along all possible directions of CMP lines. Grechka and Tsvankin (1999) showed that if the medium in the vicinity of the common midpoint is homogeneous,

$$\det\mathbf{U} = 0\,, \tag{3}$$

and the NMO-velocity surface is a cylinder. Other possible shapes include an ellipsoid and a one-sheeted hyperboloid. The NMO ellipse $\mathbf{W}$ recorded in the plane $\mathcal{P}$ can be viewed as the intersection of the NMO-velocity surface $\mathbf{U}$ with $\mathcal{P}$:

$$\mathbf{W} = \mathbf{U}\bigcap\mathcal{P}\,. \tag{4}$$

If the CMP line $\boldsymbol{\sigma}$ is curved, as in acquisition from non-flat topography (e.g., Gray et al., 1999), its curvature will influence the value of NMO velocity $V_{\rm nmo}(\boldsymbol{\sigma})$. The expression for $V_{\rm nmo}(\boldsymbol{\sigma})$ is derived in Appendix A:

$$V^{-2}_{\rm nmo}(\boldsymbol{\sigma}) = \mathcal{L}\,\mathbf{U}\,\mathcal{L}^{\mathbf{T}} + \tau_0\,\mathbf{p}\cdot\mathcal{K}\,, \tag{5}$$

where

$$\mathcal{K} = \left.\frac{d^2\boldsymbol{\sigma}(h)}{dh^2}\right|_{h=0} \tag{6}$$

is the second-order derivative of the radius-vector $\boldsymbol{\sigma}$ with respect to the half-offset h; it is evaluated at the common midpoint (zero offset). Depending on the sign of the dot product $\mathbf{p}\cdot\mathcal{K}$, the line curvature can either increase or reduce the NMO velocity.

Dix-type averaging in media with irregular interfaces

Equation (5) can be applied to CMP line $\boldsymbol{\sigma}$ that lies on any irregular surface $\mathbf{s}$. The NMO velocity $V_{\rm nmo}(\mathbf{s},\ell)$ along direction ℓ on $\mathbf{s}$ is given by equation (B9),

$$V^{-2}_{\rm nmo}(\mathbf{s},\ell) = \ell\,(\mathbf{W}+\tau_0\,\mathbf{p}\cdot\boldsymbol{\kappa})\,\ell^{\mathbf{T}}\,, \tag{7}$$

where $\mathbf{W}$ is the NMO ellipse obtained as the intersection of the NMO-velocity surface $\mathbf{U}$ with the plane $\mathcal{P}$ tangent to $\mathbf{s}$ at $\mathbf{Y}$. In equation (7) it is assumed that the slowness vector $\mathbf{p}$ is continuous across $\mathbf{s}$. The matrix

$$\boldsymbol{\kappa}_{ij} = \left.\frac{\partial^2\mathbf{s}}{\partial h_i\,\partial h_j}\right|_{h_1=h_2=0}, \qquad (i,j=1,2) \tag{8}$$

is composed of the second-order derivatives of $\mathbf{s}(h_1,\,h_2)$ with respect to the half-offsets h_1 and h_2 (Figure B1); the values $h_1=h_2=0$ correspond to the CMP location.

If $\mathbf{s}$ represents a boundary between two layers, the NMO ellipse is discontinuous across the tangent plane $\mathcal{P}$, with the jump depending on the difference between the slowness vectors above ($\mathbf{p}^{(+)}$) and below ($\mathbf{p}^{(-)}$) $\mathbf{s}$. As shown in Appendix C, equation (7) leads to the following expression for the NMO ellipse $\mathbf{W}^{(+)}$ on the "positive" side of the interface:

$$\mathbf{W}^{(+)} = \mathbf{W}^{(-)} - \tau_0\,\left(\mathbf{p}^{(+)}-\mathbf{p}^{(-)}\right)\cdot\boldsymbol{\kappa}\,, \tag{9}$$

where the term $\left[\tau_0\left(\mathbf{p}^{(+)}-\mathbf{p}^{(-)}\right)\cdot\boldsymbol{\kappa}\right]$ represents a correction for the interface curvature.

The above results make it possible to generalize the Dix-type averaging procedure of Grechka and Tsvankin (1999) to media with irregular interfaces. Suppose the model above the reflector contains N homogeneous layers, and we obtained the NMO-velocity cylinder in the layer immediately above the reflector. Slicing this cylinder by the plane tangent to the $N-1$th interface at the intersection point of the zero-offset ray yields the NMO ellipse $\mathbf{W}^{(-)}_{n-1}$. Applying equation (9), we find the ellipse $\mathbf{W}^{(+)}_{n-1}$ corrected for the interface curvature and substitute it into the Dix-type averaging equation:

$$\left[\mathbf{W}(N)\right]^{-1}\,\sum_{n=1}^{N}\tau_{0,n} = \sum_{n=1}^{N}\left[\mathbf{W}^{(+)}_n\right]^{-1}\,\tau_{0,n}\,, \tag{10}$$

where $\mathbf{W}(N)$ is the effective NMO ellipse at the earth's surface, and $\tau_{0,n}$ are the interval zero-offset traveltimes. Application of equation (10) involves projecting the NMO-velocity cylinders onto the planes tangent to the layer interfaces following the methodology of Grechka and Tsvankin (1999).

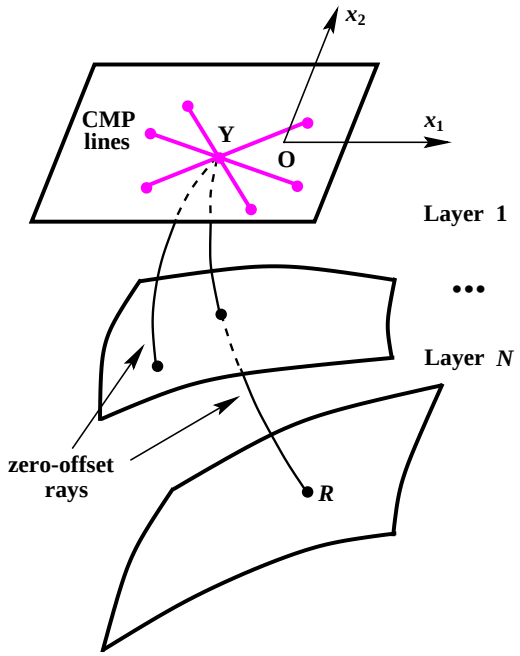

Figure 1. Multi-azimuth CMP recording over a layered VTI model with irregular interfaces.

Equation (10) allows us to compute the effective NMO ellipse $\mathbf{W}$ that can be obtained from 3-D multi-azimuth reflection data. Since it is necessary to trace only one (zero-offset) ray per common midpoint, the hyperbolic portion of pure-mode reflection moveout can be modeled without the time-consuming calculation of multi-offset and multi-azimuth traveltimes.

Parameter estimation using P-wave reflection traveltimes

Model representation and data for inversion

The above theory of NMO ellipses is a convenient tool for traveltime modeling that can be efficiently used in parameter-estimation algorithms. The inversion methodology introduced here operates exclusively with surface P-wave data acquired in wide-azimuth 3-D surveys. The input data include the zero-offset P-wave traveltimes $\tau_0(n)$, the reflection slopes in orthogonal directions (horizontal slownesses) $\mathbf{p}(n) = [p_1(n), p_2(n)]$ and the NMO ellipses $\mathbf{W}(n)$ measured for all interfaces $(n = 1, \ldots, N)$. As shown in Part I, this set of input parameters *does not* constrain the interval values of V_{P0}, ϵ and δ if the VTI layers are homogeneous and separated by planar non-intersecting boundaries. Here, however, the interfaces are allowed to be irregular, while the layers are still assumed to be homogeneous.

Our goal is to determine whether or not the data

$$\mathbf{d}(\mathbf{Y},\, n) \equiv \{\tau_0(\mathbf{Y},\, n),\, \mathbf{p}(\mathbf{Y},\, n),\, \mathbf{W}(\mathbf{Y},\, n)\}\,, \tag{11}$$

acquired at a number of CMP locations $\mathbf{Y} = [Y_1, Y_2]$ can be inverted for all relevant model parameters

$$\mathbf{m} \equiv \{V_{P0,n},\, \epsilon_n,\, \delta_n,\, \zeta_{j_1 j_2,\, n}\}\,, \tag{12}$$

$$(n = 1, \ldots, N;\; j_1 = 1, \ldots, J_1;\; j_2 = 1, \ldots, J_2)\,.$$

Here $V_{P0,n}$, ϵ_n, δ_n are the interval VTI parameters, and $\boldsymbol{\zeta}_n$ are the matrices of the coefficients describing the depths $z_n(Y_1, Y_2)$ of the model interfaces.

Since the quantities $\boldsymbol{\zeta}_n$ have to be estimated from the data, some simplification in the inversion procedure can be achieved by adopting a linear relationship between $z_n(Y_1, Y_2)$ and $\zeta_{j_1 j_2,\, n}$. In principle, this requirement can be satisfied by representing the interfaces in terms of arbitrary basis functions $B_{j_1}(Y_1)$ and $B_{j_2}(Y_2)$:

$$z_n(Y_1, Y_2) = \sum_{j_1=1}^{J_1} \sum_{j_2=1}^{J_2} \zeta_{j_1 j_2,\, n}\, B_{j_1}(Y_1)\, B_{j_2}(Y_2)\,. \tag{13}$$

For simplicity, here we elected to implement the polynomial function

$$z_n(Y_1, Y_2) = \sum_{j_1=1}^{J_1} \sum_{j_2=1}^{J_2} \zeta_{j_1 j_2,\, n}\, Y_1^{j_1 - 1}\, Y_2^{j_2 - 1}\,. \tag{14}$$

Feasibility of the inversion

For models with planar interfaces, the dependence of the data vector (11) on the CMP coordinate $\mathbf{Y}$ does not provide any new information about the model parameters (Part I). This is no longer the case in the presence of interface curvature, because zero-offset reflection rays change direction with the CMP location. Therefore, the spatial variation of the data may help to constrain the inversion and determine the depth scale of the model.

Similar to the approach outlined in Part I, the zero-offset traveltimes $\tau_0(n)$ and the reflection slopes $\mathbf{p}(n)$ can be used to find the shape of the interfaces $z_n(\mathbf{Y})$ for any given estimate of the layer parameters

$$\mathbf{l} = \{V_{P0,n},\, \epsilon_n,\, \delta_n\}\,, \quad (n = 1, \ldots, N)\,. \tag{15}$$

This is achieved by tracing zero-offset rays downward and computing the coordinates of the reflection point and the corresponding interface normal.

In contrast to media with planar interfaces, the number of common midpoints and their spatial distribution determines our ability to reconstruct the irregular interfaces. Since the slowness vector of each zero-offset ray is orthogonal to the reflector at the reflection point R (Figure 1), it provides the orientation (i.e., the azimuth and polar angle) of the unit normal $\mathbf{b}_n(R)$ to the reflecting interface. In addition, the zero-offset traveltime yields the depth of the reflection point R. Thus, the triplet $\{\tau_0(n, \mathbf{Y}),\, p_1(n, \mathbf{Y}),\, p_2(n, \mathbf{Y})\}$ at CMP location $\mathbf{Y}$ provides three constraints on the quantities $\zeta_{j_1 j_2,\, n}$ specify-

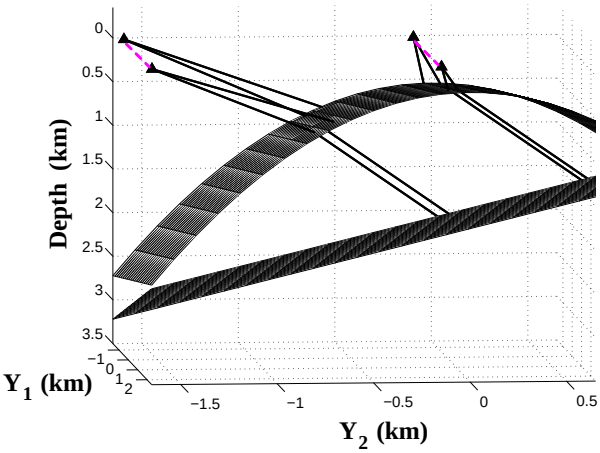

Figure 2. Zero-offset rays in the two-layer VTI model used in SVD analysis. CMP locations are marked by triangles. The relevant layer parameters are $V_{P0,1} = 1$ km/s, $\epsilon_1 = 0.20$, $\delta_1 = 0.10$, $V_{P0,2} = 2$ km/s, $\epsilon_2 = 0.15$, $\delta_2 = 0.05$. The interfaces are described by 2-D quadratic polynomials, so $\boldsymbol{\zeta}_1$ and $\boldsymbol{\zeta}_2$ are 3×3 matrices.

ing the reflector $z_n(\mathbf{Y})$ [equation (14)]. This implies that the number M of common midpoints required to obtain $J_1 \times J_2$ coefficients $\boldsymbol{\zeta}_n$ has to satisfy the inequality

$$M \geq \frac{J_1\, J_2}{3}\,. \tag{16}$$

For example, four common midpoints ($M = 4$) in Figure 2 should be sufficient for reconstructing $J_1\, J_2 = 3 \times 3 = 9$ coefficients which define each model interface. We solve the equations for the coefficients $\boldsymbol{\zeta}_n$ by least squares using all available CMP locations.

Since the traveltimes $\tau_0(n, \mathbf{Y})$ and slopes $\mathbf{p}(n, \mathbf{Y})$ are used to obtain $z_n(\mathbf{Y})$, the layer parameters $\mathbf{l}$ [equation (15)] should be found from the NMO ellipses $\mathbf{W}(n)$. To prove that the NMO ellipses may constrain the layer parameters uniquely, we present an example of singular value decomposition (SVD) analysis for a two-layer VTI model shown in Figure 2. The ellipses measured from two reflectors at four CMP locations (triangles in Figure 2) provide $2 \times 4 \times 3 = 24$ equations for the six components of the vector $\mathbf{l}$.

Thus, the feasibility of the inversion can be ascertained by applying SVD to the 24×6 matrix $\mathcal{F}$ of Frechét derivatives

$$\mathcal{F} = \frac{\partial\, \mathbf{W}(n, \mathbf{Y})}{\partial\, \mathbf{l}} \tag{17}$$

computed for correct values of model parameters $\mathbf{m}$. Since none of the singular values vanishes (Figure 3), the input data provide sufficient information for parameter estimation, and this VTI model can be fully reconstructed in the depth domain from P-wave reflection traveltimes.

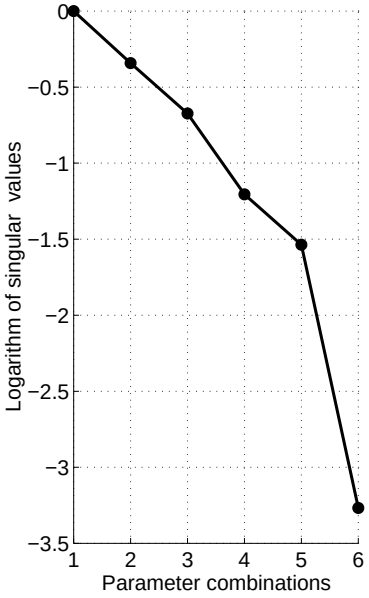

Figure 3. Normalized singular values for the model from Figure 2.

Clearly, it is not *always* possible to obtain VTI parameters using just P-wave data. For example, as the curvature of the intermediate interface in Figure 2 decreases, our model approaches that with planar interfaces where at least one singular value is zero (Part I). One of the singular values also vanishes when either layer is elliptically anisotropic, so that $\epsilon_n = \delta_n$ (Dellinger and Muir, 1988).

Numerical examples

To confirm the SVD results, we carried out actual inversion of P-wave data for the model in Figure 2 in the presence of noise. Reflection traveltimes were computed for 240 common midpoints placed at every 25 m along the two dashed lines between the triangles in Figure 3. This provided an overdetermined system of $240 \times 3 = 720$ equations for reconstructing the interface parameters $\boldsymbol{\zeta}_n$. We added Gaussian noise to the modeled NMO velocities and zero-offset traveltimes and obtained the parameter vector $\mathbf{m}$ [equation (12)] using least-squares fitting of the data $\mathbf{d}$ [equation (11)]. Comparing the results of this test with the actual parameters (Table 1), we conclude that all three parameters in both layers were found with good accuracy. The relative errors in the interval vertical velocities $V_{P0,n}$ and absolute errors in the anisotropic coefficients are comparable to the standard deviation of the noise added to the NMO velocities. The inversion results do not depend (for the same input data) on the initial guess for the model parameters, which suggests that the least-squares objective function in a certain vicinity of the correct solution is unimodal. Knowledge of the in-

	$V_{P0,1}$ (km/s)	ϵ_1	δ_1	$V_{P0,2}$ (km/s)	ϵ_2	δ_2
Correct	1.00	0.20	0.10	2.00	0.15	0.05
Inverted	1.02	0.17	0.07	2.05	0.11	0.03

Table 1. Inversion results for the two-layer VTI model from Figure 2. The standard deviations of Gaussian noise added to the NMO velocities and zero-offset traveltimes are 2.0% and 1.0%, respectively.

	$V_{P0,1}$ (km/s)	ϵ_1	δ_1	$V_{P0,2}$ (km/s)	ϵ_2	δ_2	$V_{P0,3}$ (km/s)	ϵ_3	δ_3
Correct	1.80	0.20	0.10	2.00	0.15	0.05	2.30	0.10	0.03
Inverted	1.77	0.23	0.12	1.97	0.17	0.07	2.26	0.12	0.05

Table 2. Inversion results for the three-layer VTI model from Figure 4. The errors in the inverted quantities are due to Gaussian noise added to the zero-offset traveltimes and NMO velocities. The standard deviations of the noise are 1.0% (for the traveltimes) and 2.0% (for the velocities).

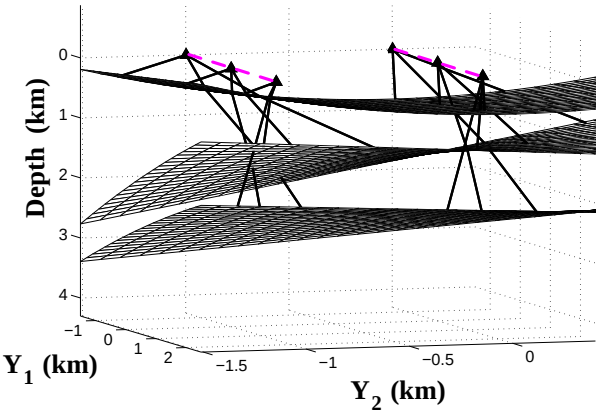

Figure 4. The three-layer VTI model used in the inversion with several zero-offset rays. Common midpoints are located on the two gray dashed lines.

terval VTI parameters $V_{P0,n}$, ϵ_n and δ_n is sufficient to reconstruct the depth and shape of the interfaces and build the whole VTI model *in depth*.

Another example, this time for a three-layer VTI model with a more complicated shape of the interfaces is shown in Figure 4 and Table 2. The data vector $\mathbf{d}(\mathbf{Y}, n)$ was determined from the traveltimes computed at 600 common midpoints located along two lines with a spacing of 15 m. The accuracy of parameter estimation on noise-contaminated data (Table 2) is comparable to that in the example from Table 1. Therefore, for a subset of layered VTI models with irregular interfaces, P-wave reflection traveltimes provide sufficient information for the inversion in the depth domain.

Discussion and conclusions

The possibility of inverting P-wave reflection data for the interval parameters of layered VTI media strongly depends on the geometry of intermediate interfaces. While only the zero-dip NMO velocity $V_{\rm nmo}(0)$ and η can be obtained for laterally homogeneous VTI media above the reflector, the presence of dipping or irregular interfaces may help to estimate all three relevant anisotropic parameters (V_{P0}, ϵ and δ). For planar interfaces which do not intersect each other, unambiguous inversion requires *a priori* knowledge of a single interval VTI parameter in at least one layer (Part I).

Here we discussed P-wave moveout inversion for more complicated VTI media with irregular interfaces. To compute azimuthally dependent NMO velocity in such models, we extended the theory of NMO-velocity surfaces (Grechka and Tsvankin, 1999) by deriving a correction for the interface curvature. The new methodology generates NMO ellipses over arbitrary anisotropic media with irregular interfaces by tracing a *single* zero-offset ray per CMP. This modeling algorithm, which is several orders of magnitude faster than 3-D two-point ray tracing, provides a foundation for efficient traveltime inversion.

The feasibility of the interval parameter estimation was studied using singular value decomposition (SVD) followed by the tomographic-style inversion of noise-contaminated data. The input parameters for the inversion include P-wave zero-offset traveltimes and azimuthally dependent NMO velocities (i.e., NMO ellipses) acquired at a number of common midpoints over the study area. In contrast to media with planar interfaces discussed in Part I, for a subset of VTI models with ir-

regular interfaces it is possible to reconstruct the model in depth from P-wave reflection traveltimes alone. Interface curvature increases the angle coverage of reflected rays, which helps to constrain the parameters of the anisotropic velocity field. Only if the anisotropy of one or more layers is close to elliptical, the depth scale becomes poorly constrained by P-wave data regardless of the interface shape, which agrees with the results of Dellinger and Muir (1988).

The most critical assumption that ensured the success of the inversion procedure is that the model is composed of *homogeneous* layers. Allowing for a variation in the VTI parameters within some of the layers may prevent us from resolving the three principal components of the model: anisotropy, irregular interfaces and lateral velocity variation. Even for isotropic models with irregular interfaces and laterally varying velocity, the traveltime inversion is generally nonunique (Goldin, 1986). Still, in some special cases it may be possible to separate the contributions of each of those three factors to the reflection traveltimes; this topic requires further investigation.

Acknowledgments

We are grateful to members of the A(nisotropy)-Team at the Center for Wave Phenomena (CWP), Colorado School of Mines, for helpful discussions and Ken Larner (CSM) for his review of the manuscript. The support for this work was provided by the members of the Consortium Project on Seismic Inverse Methods for Complex Structures at CWP and by the United States Department of Energy (Award #DE-FG03-98ER14908).

References

Alkhalifah, T., and Tsvankin, I., 1995, Velocity analysis in transversely isotropic media: Geophysics, **60**, 1550–1566.

Chernyak, V.S., and Gritsenko, S.A., 1979, Interpretation of effective parameters of the CDP-method for system of 3-D homogeneous layers separated by irregular interfaces: Geology and Geophysics, **12**, 112–120 (in Russian).

Dellinger, J., and Muir, F., 1988, Imaging reflections in elliptically anisotropic media: Geophysics, **53**, 1616–1618.

Goldin, S.V., 1986, Seismic traveltime inversion: Soc. Expl. Geophys.

Gray, S.H., Maclean, G., and Marfurt, K.J., 1999, Crooked line, rough topography: advancing towards the correct seismic image: Geophys. Prosp., **47**, 721–733.

Grechka, V., Pech, A., and Tsvankin, I., 2000, Inversion of P-wave data in laterally heterogeneous VTI media. Part I: Plane dipping interfaces: This volume.

Grechka, V., and Tsvankin, I., 1998, 3-D description of normal moveout in anisotropic inhomogeneous media: Geophysics, **63**, 1079-1092.

Grechka, V., and Tsvankin, I., 1999, NMO surfaces and Dix-type formulae in heterogeneous anisotropic media: 69th Ann. Internat. Mtg., Soc. Expl. Geophys., Expanded Abstracts, 1612–1615.

Grechka, V., Tsvankin, I., and Cohen, J.K., 1999, Generalized Dix equation and analytic treatment of normal-moveout velocity for anisotropic media: Geophys. Prosp., **47**, 117–148.

Hubral, P., and Krey, T., 1980, Interval velocities from seismic reflection measurements: Soc. Expl. Geophys.

Le Stunff, Y., Grechka, V., and Tsvankin, I., 1999, Depth-domain velocity analysis in VTI media using surface P-wave data: Is it feasible? 69th Ann. Internat. Mtg., Soc. Expl. Geophys., Expanded Abstracts, 1604–1607.

Thomsen, L., 1986, Weak elastic anisotropy: Geophysics, **51**, 1954–1966.

Tsvankin, I., and Grechka, V., 2000, Dip moveout of converted waves and parameter estimation in transversely isotropic media: Geophys. Prosp., **48**, 257–292.

APPENDIX A: NMO velocity along a curved CMP line

Here we extend the derivation of the NMO velocity measured along a *straight* arbitrarily oriented CMP line given by Grechka and Tsvankin (1999) to CMP lines with nonzero curvature at the common midpoint. Our derivation is based on expanding the pure-mode reflection traveltime t in a Taylor series in half offset h ($h = 0$ at the CMP location). The traveltime is assumed to be smooth enough for all needed derivatives to exist at zero offset.

Let us denote $\mathbf{x}_{\rm CMP} = \boldsymbol{\sigma}(0)$ the coordinate of the common midpoint O (Figure A1) on the irregular CMP line $\boldsymbol{\sigma}$. If the CMP line is parameterized as a function of its arclength h, the coordinates of the source S and receiver R become $\boldsymbol{\sigma}(-h)$ and $\boldsymbol{\sigma}(h)$. Since we are interested in the small-offset approximation of the reflection traveltime, the function $\boldsymbol{\sigma}(h)$ can be replaced by its quadratic Taylor series expansion in the vicinity of $h = 0$:

$$\boldsymbol{\sigma}(h) = \mathbf{x}_{\rm CMP} + \mathcal{L}\,h + \frac{1}{2}\,\mathcal{K}\,h^2 + o(h^2)\,. \tag{A1}$$

Here $\mathcal{L}$ is the unit vector tangent to the CMP line at $h = 0$,

$$\mathcal{L} \equiv \left.\frac{d\boldsymbol{\sigma}}{dh}\right|_{h=0}, \tag{A2}$$

and $\mathcal{K}$ is related to the curvature of the CMP line,

$$\mathcal{K} \equiv \left.\frac{d^2\boldsymbol{\sigma}}{dh^2}\right|_{h=0}. \tag{A3}$$

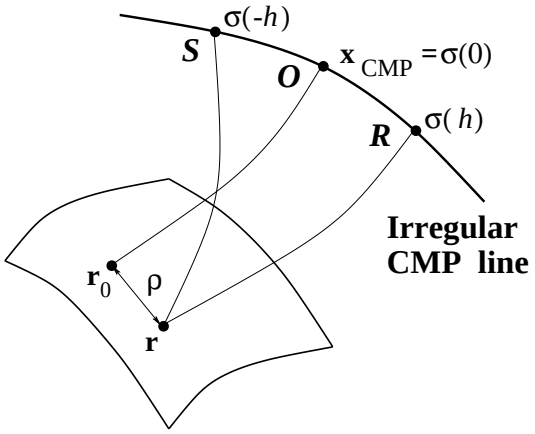

Figure A1. Reflection traveltimes are recorded along the curved CMP line $\boldsymbol{\sigma}$ with the common midpoint at O. Note the difference between the reflection points $\mathbf{r}_0$ and $\mathbf{r}$ of the zero-offset and nonzero-offset rays.

The pure-mode two-way reflection traveltime t measured at small offsets h along the CMP line $\boldsymbol{\sigma}$ can be expanded in a similar quadratic Taylor series,

$$t\Big(\boldsymbol{\sigma}(h),\mathbf{r}\Big) = t\Big(\boldsymbol{\sigma}(0),\mathbf{r}\Big) + \left.\frac{dt\Big(\boldsymbol{\sigma}(h),\mathbf{r}\Big)}{dh}\right|_{h=0} h + \frac{1}{2}\left.\frac{d^2t\Big(\boldsymbol{\sigma}(h),\mathbf{r}\Big)}{dh^2}\right|_{h=0} h^2 + \ldots \tag{A4}$$

The traveltime t depends on the source and receiver positions and on the coordinate $\mathbf{r}$ of the reflection point. Summing up the one-way traveltimes τ corresponding to the down- and upgoing rays, we can write

$$t\Big(\boldsymbol{\sigma}(h),\mathbf{r}\Big) = \tau\Big(\boldsymbol{\sigma}(-h),\mathbf{r}\Big) + \tau\Big(\boldsymbol{\sigma}(h),\mathbf{r}\Big)\,. \tag{A5}$$

We begin with showing (following the derivation of Tsvankin and Grechka, 2000) that the reflection point dispersal (i.e., the deviation of $\mathbf{r}$ from the zero-offset reflection point $\mathbf{r}_0$ in Figure A1) has no influence on the values of the derivatives dt/dh and d^2t/dh^2 at $h=0$, so equation (A5) can be replaced with

$$t\Big(\boldsymbol{\sigma}(h),\mathbf{r}\Big) = t\Big(\boldsymbol{\sigma}(h),\mathbf{r}_0\Big) = \tau\Big(\boldsymbol{\sigma}(-h),\mathbf{r}_0\Big) + \tau\Big(\boldsymbol{\sigma}(h),\mathbf{r}_0\Big)\,. \tag{A6}$$

Let us examine the difference

$$\Delta t \equiv t\Big(\boldsymbol{\sigma}(h),\mathbf{r}\Big) - t\Big(\boldsymbol{\sigma}(h),\mathbf{r}_0\Big)\,\Big|_{\text{fixed }\boldsymbol{\sigma}\text{ and }h} \tag{A7}$$

between the traveltimes corresponding to the specular reflection point $\mathbf{r}$ and to the zero-offset (non-specular) reflection point $\mathbf{r}_0$. The source and receiver are located along the CMP line $\boldsymbol{\sigma}$ at the fixed half-offset h. The difference Δt can be expanded in a Taylor series in the distance $\rho = |\mathbf{r}-\mathbf{r}_0|$ between the points $\mathbf{r}$ and $\mathbf{r}_0$ (Figure A1). At zero-offset, $\mathbf{r}=\mathbf{r}_0$ and $\Delta t|_{\rho=0} = 0$ as follows from equation (A7). Since the traveltime has an extremum at the specular reflection point $\mathbf{r}$ (Fermat's principle), the series $\Delta t(\rho)$ starts with the quadratic term

$$\Delta t(\rho) = \frac{1}{2}\,A\Big(\boldsymbol{\sigma}(h)\Big)\,\rho^2\Big(\boldsymbol{\sigma}(h)\Big) + o(\rho^2)\,, \tag{A8}$$

where

$$A\Big(\boldsymbol{\sigma}(h)\Big) = -\left.\frac{d^2t\Big(\boldsymbol{\sigma}(h),\mathbf{r}\Big)}{d\rho^2}\right|_{\mathbf{r}}\,. \tag{A9}$$

Differentiating equation (A8) with respect to h yields

$$\frac{d\Delta t}{dh} = \frac{dA\Big(\boldsymbol{\sigma}(h)\Big)}{dh}\,\rho^2\Big(\boldsymbol{\sigma}(h)\Big) + 2\,A\Big(\boldsymbol{\sigma}(h)\Big)\,\rho\Big(\boldsymbol{\sigma}(h)\Big)\,\frac{d\rho\Big(\boldsymbol{\sigma}(h)\Big)}{dh}\,. \tag{A10}$$

Since $\rho = 0$ at $h=0$, the derivative

$$\left.\frac{d\Delta t}{dh}\right|_{h=0} = 0\,. \tag{A11}$$

Therefore,

$$\left.\frac{dt\Big(\boldsymbol{\sigma}(h),\mathbf{r}\Big)}{dh}\right|_{h=0} = \left.\frac{dt\Big(\boldsymbol{\sigma}(h),\mathbf{r}_0\Big)}{dh}\right|_{h=0}\,. \tag{A12}$$

Next, we differentiate equation (A10) again:

$$\begin{aligned}\frac{d^2\Delta t}{dh^2} = {} & \frac{d^2A\Big(\boldsymbol{\sigma}(h)\Big)}{dh^2}\,\rho^2\Big(\boldsymbol{\sigma}(h)\Big) + 4\,\frac{dA\Big(\boldsymbol{\sigma}(h)\Big)}{dh}\,\rho\Big(\boldsymbol{\sigma}(h)\Big)\,\frac{d\rho\Big(\boldsymbol{\sigma}(h)\Big)}{dh} \\ & +2\,A\Big(\boldsymbol{\sigma}(h)\Big)\left[\frac{d\rho\Big(\boldsymbol{\sigma}(h)\Big)}{dh}\right]^2 + 2\,A\Big(\boldsymbol{\sigma}(h)\Big)\,\rho\Big(\boldsymbol{\sigma}(h)\Big)\,\frac{d^2\rho\Big(\boldsymbol{\sigma}(h)\Big)}{dh^2}\,.\end{aligned} \tag{A13}$$

Evaluating the derivative (A13) at $h = \rho = 0$, we obtain

$$\left.\frac{d^2\Delta t}{dh^2}\right|_{h=0} = 2\,A\Big(\boldsymbol{\sigma}(h)\Big)\left[\frac{d\rho\Big(\boldsymbol{\sigma}(h)\Big)}{dh}\right]^2\Bigg|_{h=0}\,. \tag{A14}$$

To show that the derivative (A14) is zero, we note that both the traveltime and the ray trajectory of a pure reflection mode remain the same if we interchange the source and receiver positions (the reciprocity principle). Hence,

$$\mathbf{r}\Big(\boldsymbol{\sigma}(h)\Big) = \mathbf{r}\Big(\boldsymbol{\sigma}(-h)\Big) \tag{A15}$$

and, therefore,

$$\rho\Big(\boldsymbol{\sigma}(h)\Big) \equiv \Big|\mathbf{r}\Big(\boldsymbol{\sigma}(h)\Big) - \mathbf{r}_0\Big| = \Big|\mathbf{r}\Big(\boldsymbol{\sigma}(-h)\Big) - \mathbf{r}_0\Big| = \rho\Big(\boldsymbol{\sigma}(-h)\Big)\,, \tag{A16}$$

i.e., ρ is an even function of h for any fixed CMP line $\boldsymbol{\sigma}$. Consequently,

$$\left.\frac{d\rho\Big(\boldsymbol{\sigma}(h)\Big)}{dh}\right|_{h=0} = 0\,, \tag{A17}$$

so equation (A14) results in

$$\left.\frac{d^2\Delta t}{dh^2}\right|_{h=0} = 0\,. \tag{A18}$$

Thus, we have proven that

$$\left.\frac{d^2t\Big(\boldsymbol{\sigma}(h),\mathbf{r}\Big)}{dh^2}\right|_{h=0} = \left.\frac{d^2t\Big(\boldsymbol{\sigma}(h),\mathbf{r}_0\Big)}{dh^2}\right|_{h=0}\,, \tag{A19}$$

and the derivatives in the series (A4) can be obtained by differentiating equation (A6). This result is equivalent to the normal incidence point (NIP) theorem proved by Chernyak and Gritsenko (1979) (their proof can be also found in Goldin, 1986) and by Hubral and Krey (1980).

The zero-offset ($h = 0$) traveltime can be expressed as [see equation (A6)]

$$t\Big(\boldsymbol{\sigma}(h),\mathbf{r}_0\Big)\Big|_{h=0} \equiv t_0 = 2\,\tau(\mathbf{x}_{\rm CMP}). \tag{A20}$$

Differentiating equation (A6) and taking into account equation (A1), we find

$$\left.\frac{dt\Big(\boldsymbol{\sigma}(h)\Big)}{dh}\right|_{h=0} = \sum_{k=1}^{3}\frac{\partial\tau}{\partial\sigma_k}\Big(-\mathcal{L}_k + \mathcal{L}_k + 2\,\mathcal{K}_k\,h + o(h)\Big)\Big|_{h=0} = 0\,. \tag{A21}$$

Differentiating the one-way traveltime with respect to h twice yields

$$\frac{d^2\tau\Big(\boldsymbol{\sigma}(h)\Big)}{dh^2} = \sum_{k,m=1}^{3} \frac{\partial^2\tau\Big(\boldsymbol{\sigma}(h)\Big)}{\partial\sigma_k\,\partial\sigma_m}\,\frac{d\sigma_k}{dh}\,\frac{d\sigma_m}{dh} + \sum_{k=1}^{3} \frac{\partial\tau\Big(\boldsymbol{\sigma}(h)\Big)}{\partial\sigma_k}\,\frac{d^2\sigma_k}{dh^2}\,. \tag{A22}$$

Using equations (A1), (A6) and (A22) leads to

$$\left.\frac{d^2t\Big(\boldsymbol{\sigma}(h)\Big)}{dh^2}\right|_{h=0} = 2\sum_{k,m=1}^{3} \left.\frac{\partial^2\tau\Big(\boldsymbol{\sigma}(h)\Big)}{\partial\sigma_k\,\partial\sigma_m}\right|_{h=0} \mathcal{L}_k\,\mathcal{L}_m + 2\sum_{k=1}^{3} \left.\frac{\partial\tau\Big(\boldsymbol{\sigma}(h)\Big)}{\partial\sigma_k}\right|_{h=0} \mathcal{K}_k\,. \tag{A23}$$

Noting that

$$\left.\frac{\partial}{\partial\sigma_k}\right|_{h=0} = \left.\frac{\partial}{\partial x_k}\right|_{h=0} \tag{A24}$$

equation (A23) can be rewritten in the following form:

$$\left.\frac{d^2t\Big(\boldsymbol{\sigma}(h)\Big)}{dh^2}\right|_{h=0} = 2\sum_{k,m=1}^{3} \left.\frac{\partial^2\tau(\mathbf{x})}{\partial x_k\,\partial x_m}\right|_{h=0} \mathcal{L}_k\,\mathcal{L}_m + 2\sum_{k=1}^{3} \left.\frac{\partial\tau(\mathbf{x})}{\partial x_k}\right|_{h=0} \mathcal{K}_k\,. \tag{A25}$$

Equation (A25) relates the second-order derivative of the two-way traveltime t with respect to the half-offset and the second-order spatial derivatives of the one-way traveltime τ from the zero-offset reflection point.

To obtain an equation for the NMO velocity along the CMP line $\boldsymbol{\sigma}$, we substitute the derivatives (A21) and (A25) into the series (A4):

$$t\Big(\boldsymbol{\sigma}(h)\Big) = t_0 + h^2 \left\{ \sum_{k,m=1}^{3} \left.\frac{\partial^2\tau(\mathbf{x})}{\partial x_k\,\partial x_m}\right|_{h=0} \mathcal{L}_k\,\mathcal{L}_m + \sum_{k=1}^{3} \left.\frac{\partial\tau(\mathbf{x})}{\partial x_k}\right|_{h=0} \mathcal{K}_k \right\}. \tag{A26}$$

Squaring this equation and keeping the quadratic and lower-order terms with respect to h yields

$$t^2\Big(\boldsymbol{\sigma}(h)\Big) = t_0^2 + 2\,t_0\,h^2 \left\{ \sum_{k,m=1}^{3} \left.\frac{\partial^2\tau(\mathbf{x})}{\partial x_k\,\partial x_m}\right|_{h=0} \mathcal{L}_k\,\mathcal{L}_m + \sum_{k=1}^{3} \left.\frac{\partial\tau(\mathbf{x})}{\partial x_k}\right|_{h=0} \mathcal{K}_k \right\}. \tag{A27}$$

Introducing the source-receiver offset

$$X = 2\,h\,, \tag{A28}$$

we rewrite equation (A27) in its final form,

$$t^2\Big(\boldsymbol{\sigma}(X)\Big) = t_0^2 + (\mathcal{L}\,\mathbf{U}\,\mathcal{L}^{\mathbf{T}} + \tau_0\,\mathbf{p}\cdot\mathcal{K})\,X^2\,, \tag{A29}$$

where $\tau_0 = t_0/2$ is the one-way zero-offset traveltime. Here $\mathbf{T}$ denotes transposition, and the 3×3 symmetric matrix $\mathbf{U}$ is defined as

$$U_{km} \equiv \tau_0\,\left.\frac{\partial^2\tau(\mathbf{x})}{\partial x_k\,\partial x_m}\right|_{h=0} = \tau_0\,\left.\frac{\partial p_k(\mathbf{x})}{\partial x_m}\right|_{h=0}, \qquad (k,m=1,2,3)\,; \tag{A30}$$

$$p_k(\mathbf{x}) \equiv \frac{\partial\tau(\mathbf{x})}{\partial x_k}\,, \qquad (k,m=1,2,3), \tag{A31}$$

are the components of the slowness vector $\mathbf{p}=[p_1,p_2,p_3]$. In equation (A29) $\mathbf{p}$ is evaluated at the CMP location.

Comparing equation (A29) with the conventional definition of the NMO velocity $V_{\rm nmo}(\boldsymbol{\sigma})$ along the CMP line $\boldsymbol{\sigma}$,

$$t^2\Big(\boldsymbol{\sigma}(X)\Big) = t_0^2 + \frac{X^2}{V_{\rm nmo}^2(\boldsymbol{\sigma})}\,, \tag{A32}$$

we conclude that

$$V_{\rm nmo}^{-2}(\boldsymbol{\sigma}) = \mathcal{L}\,\mathbf{U}\,\mathcal{L}^{\mathbf{T}} + \tau_0\,\mathbf{p}\cdot\mathcal{K}\,. \tag{A33}$$

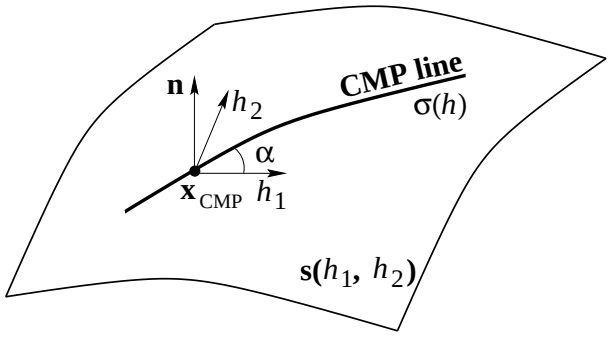

Figure B1. CMP line $\boldsymbol{\sigma}$ at an irregular surface described by the radius-vector $\mathbf{s}(h_1, h_2)$. $\mathbf{n}$ is the unit vector orthogonal to the surface at common midpoint $\mathbf{x}_{\mathrm{CMP}}$.

APPENDIX B: NMO velocity at an irregular surface

Equation (A33) can be used to describe the azimuthal variation of the NMO velocity measured along CMP lines at an irregular surface $\mathbf{s}$. Let us specify the surface

$$\mathbf{s} \equiv \mathbf{s}(h_1, h_2) \tag{B1}$$

by a pair of curvilinear orthogonal coordinates h_1 and h_2 (Figure B1) in such a way that the half-offset h along the CMP line $\boldsymbol{\sigma}$ is given as (for $h \to 0$)

$$h_1 = h \cos\alpha \tag{B2}$$

and

$$h_2 = h \sin\alpha\,, \tag{B3}$$

where α is the azimuth of the tangent to the CMP line at the common midpoint $\mathbf{x}_{\mathrm{CMP}}$ with respect to the axis h_1 (Figure B1).

For simplicity, the axis x_3 of the coordinate frame is directed along the normal $\mathbf{n}$ to the surface $\mathbf{s}(h_1, h_2)$ at the CMP location. This implies that the tangent vector $\mathcal{L}$ to the CMP line at $\mathbf{x}_{\mathrm{CMP}}$ [see equation (A2)] is

$$\mathcal{L} = [\cos\alpha,\, \sin\alpha,\, 0]\,, \tag{B4}$$

and we can replace $\mathcal{L}$ with the vector ℓ which lies in $\mathbf{s}$:

$$\ell \equiv [\mathcal{L}_1,\, \mathcal{L}_2] = [\cos\alpha,\, \sin\alpha]\,. \tag{B5}$$

To obtain the NMO velocity for any CMP line $\boldsymbol{\sigma}$ within $\mathbf{s}$, we need to express the curvature $\mathcal{K}$ in equation (A33) in terms of the derivatives of $\mathbf{s}$ with respect to the coordinates h_1 and h_2. Using equations (A3), (B2) and (B3), we find

$$\mathcal{K} = \left.\frac{d^2\mathbf{s}}{dh^2}\right|_{\text{along }\boldsymbol{\sigma},\ h=0} = \left.\sum_{i,j=1}^{2} \frac{\partial^2\mathbf{s}}{\partial h_i\,\partial h_j}\,\frac{dh_i}{dh}\,\frac{dh_j}{dh}\right|_{h=0}$$
$$= \boldsymbol{\kappa}_{11}\cos^2\alpha + 2\,\boldsymbol{\kappa}_{12}\sin\alpha\cos\alpha + \boldsymbol{\kappa}_{22}\sin^2\alpha\,, \tag{B6}$$

where

$$\boldsymbol{\kappa}_{ij} \equiv \left.\frac{\partial^2\mathbf{s}}{\partial h_i\,\partial h_j}\right|_{h_1=h_2=0}, \qquad (i,j=1,2)\,. \tag{B7}$$

Equation (B6) can be rewritten in matrix form using equation (B5):

$$\mathcal{K} = \ell\,\boldsymbol{\kappa}\,\ell^{\mathbf{T}}\,. \tag{B8}$$

Equation (A33) then yields

$$V_{\mathrm{nmo}}^{-2}(\mathbf{s},\ell) = \ell\,(\mathbf{W} + \tau_0\,\mathbf{p}\cdot\boldsymbol{\kappa})\,\ell^{\mathbf{T}}\,, \tag{B9}$$

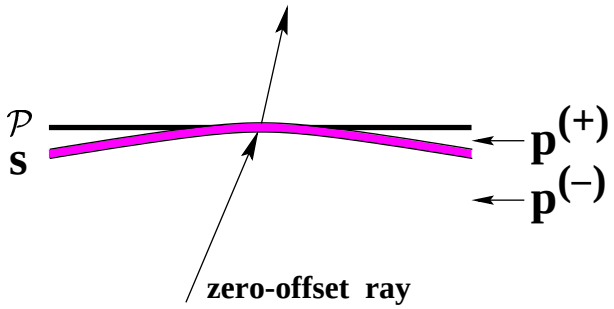

Figure C1. Zero-offset ray crossing an irregular interface **s**. Plane $\mathcal{P}$ is tangent to the interface at the intersection point; $\mathbf{p}^{(+)}$ and $\mathbf{p}^{(-)}$ are the slowness vectors on different sides of the interface.

where

$$W_{ij} \equiv U_{ij}\,, \qquad (i,j=1,2)\,. \tag{B10}$$

Thus, the directional dependence of the NMO velocity $V_{\rm nmo}(\mathbf{s},\ell)$ measured on the irregular surface **s** can be described in terms of the following 2×2 symmetric quadratic form:

$$\mathcal{W} \equiv \mathbf{W} + \tau_0\,\mathbf{p}\cdot\boldsymbol{\kappa}\,, \tag{B11}$$

where $\mathbf{W}$ is the matrix that represents the NMO ellipse in the plane tangent to **s** at the CMP location, and $\tau_0\,\mathbf{p}\cdot\boldsymbol{\kappa}$ is the correction for the curvature.

APPENDIX C: Continuation of NMO velocities through irregular interfaces

Grechka and Tsvankin (1999) developed concise Dix-type formulae for anisotropic models composed of homogeneous layers separated by planar interfaces. They showed that the effective NMO ellipse at a given CMP location can be obtained by averaging the intersections of the NMO-velocity surfaces with the layer boundaries along the zero-offset ray. Here, we use the results of Appendices A and B to extend their procedure to media with irregular interfaces.

The derivation of Grechka and Tsvankin (1999) was based on the fact that the intersections of the NMO-velocity surfaces $\mathbf{U}$ with the planar boundaries (i.e., the NMO ellipses $\mathbf{W}$) are the same on both sides of each interface. For irregular interfaces, the quantities continuous across the interfaces are the matrices $\mathcal{W}$ defined by equation (B11). Indeed, $\mathcal{W}$ determine the NMO velocities measured on the top (+) and bottom (−) sides of the interface **s** (Figure C1). According to equation (B11),

$$\mathcal{W}^{(+)} = \mathbf{W}^{(+)} + \tau_0\,\mathbf{p}^{(+)}\cdot\boldsymbol{\kappa}\,, \tag{C1}$$

$$\mathcal{W}^{(-)} = \mathbf{W}^{(-)} + \tau_0\,\mathbf{p}^{(-)}\cdot\boldsymbol{\kappa}\,. \tag{C2}$$

As shown in Appendix A, NMO velocity can be computed using the one-way traveltimes from the zero-offset reflection point to the CMP line. Essentially, those traveltimes correspond to the wavefront propagating from the zero-offset reflection point. To satisfy the boundary conditions, the wavefront has to be continuous across surface **s**, which implies that the NMO velocities measured on two sides of **s** at the reflection/transmission point (Figure C1) are identical. Therefore,

$$\mathcal{W}^{(+)} = \mathcal{W}^{(-)}\,. \tag{C3}$$

In contrast, the NMO ellipses $\mathbf{W}^{(+)}$ and $\mathbf{W}^{(-)}$ measured on two sides of the plane $\mathcal{P}$ tangent to **s** have to be different because the slowness vector changes across the interface. Combining equations (C1)–(C3), we find

$$\mathbf{W}^{(+)} = \mathbf{W}^{(-)} - \tau_0\,\left(\mathbf{p}^{(+)} - \mathbf{p}^{(-)}\right)\cdot\boldsymbol{\kappa}\,. \tag{C4}$$

As discussed in the main text, the correction of NMO ellipses for the interface curvature developed here can be used to extend the Dix-type averaging formulae of Grechka et al. (1999) and Grechka and Tsvankin (1999) to media with irregular interfaces.